2023

An Adaptive Vector Control Method For Inverter-Based Stand-Alone Microgrids Considering Voltage Reduction And Load Shedding Schemes

Sumit Kumar Jha
Birla Institute of Technology, Mesra, Ranchi, India

Deepak Kumar
Birla Institute of Technology, Mesra, Ranchi, India

Prabhat Ranjan Tripathi
Birla Institute of Technology, Mesra, Ranchi, India

See next page for additional authors

Funder: This research received no external funding

Received: 31 December 2022 | Revised: 7 January 2023 | Accepted: 22 March 2023

IET Generation, Transmission & Distribution

DOI: 10.1049/gtd2.12839

The Institution of Engineering and Technology WILEY

ORIGINAL RESEARCH

An adaptive vector control method for inverter-based stand-alone microgrids considering voltage reduction and load shedding schemes

Sumit Kumar Jha[1,2] | **Deepak Kumar**[1] | **Prabhat Ranjan Tripathi**[1] | **Bhargav Appasani**[3] | **Hossam M. Zawbaa**[4,5,6] | **Salah Kamel**[7]

[1]Department of Electrical and Electronics Engineering, Birla Institute of Technology, Mesra, Ranchi, India

[2]Department of Electrical and Electronics Engineering, Presidency University, Bengaluru, Karnataka, India

[3]School of Electronics Engineering, Kalinga Institute of Industrial Technology, Bhubaneswar, India

[4]Faculty of Computers and Artificial Intelligence, Beni-Suef University, Beni-Suef, Egypt

[5]CeADAR - Ireland's Centre for AI and Applied Data Analytics, Technological University Dublin, Dublin, Ireland

[6]Applied Science Research Center, Applied Science Private University, Amman, Jordan

[7]Electrical Engineering Department, Faculty of Engineering, Aswan University, Aswan, Egypt

Correspondence
Hossam M. Zawbaa, Technological University Dublin, Park House, 191 N Circular Rd, Cabra East, Grangegorman, Dublin D07 EWV4, Ireland.
Email: hossam.zawbaa@gmail.com

Abstract

The droop mechanism is widely utilized in a stand-alone microgrid (MG) to regulate power-sharing among distributed generators (DG). However, over the years, the droop phenomena are continually modified to lessen the deviation in voltage and frequency parameters caused due to classical droop. This study suggests computing the droop coefficient for voltage–current (V–I) droop to take into account for proportional power distribution among DGs. In grid utility networks, the conservation voltage reduction (CVR) strategy is widely used to curtail the use of energy. Hence, this paper investigates the CVR's performance for stand-alone MG by performing the adaptive vector control scheme in the two-phase d–q reference frame. In addition to it, the paper is intended to develop a coordinated control strategy for stand-alone MG involving classical P–f droop and self-sustained V–I droop employed to perform the function of CVR during peak demand and overloading conditions. Further, a load-shedding control approach is also considered to cut out some segments of load during overloading conditions to operate the MG in the stable zone. The validation of the proposed strategy is conducted on MATLAB/Simulink software.

1 | INTRODUCTION

The paradigm shifts from the conventional power system to the inverter-based distributed generator (DG) led to increased penetration of renewable sources in the distributed power network [1]. Microgrid (MG) emerges out to be the distinctive technology that enables large integration of distributed generation with sophisticated control mechanism [2]. The centralized and decentralized control are the two schemes that are widely practiced in the control approach of MG. The centralized control scheme is dependent on a communication wire to pass the control and feedback signal and hence, decentralized control is most commonly used for power sharing among DGs. The P–f and Q–E are the two variants of the droop control scheme that are widely used as a decentralized approach to maintaining the power among DGs. The P–f/Q–E approach relies on the inductive network, and it suffers slow dynamic issues with an abrupt change of voltage and frequency parameters as the load drifts to a new position [3]. In addition to it, the droop coefficient determination in the conventional droop method is decided by assuming the proper power balance between the DG and the load demand whereas the work proposed in [4]

illustrated the droop coefficient estimation as per the power output of the solar PV. An AC–DC coupled droop control mechanism is proposed in [5] to eliminate outer controller loops consisting of PI controller to facilitate fast dynamics of the bus voltage during the time of transients.

Microgrid characterizes line impedance of resistive nature, and its DG is having least inertia with frequent load variation, hence, the stability and power quality are the challenging issues for the droop control scheme. Various literature addressed these challenges and contributed to the design of robust control mechanisms. A control strategy comprising the model predictive control is utilized to adjust the gain of the droop controller and voltage reference of the DGs to regulate the frequency of the system within the predetermined limits [6]. A detailed review illustration of various kinds of control methods implemented in hierarchical control and the techniques for frequency and voltage restoration is discussed in [7]. The voltage control of the battery energy storage system is carried out with the coordination of *P–f* and *V–I* droop control to regulate the charging phenomena of the battery energy storage system proposed in [8]. In [9], the overshoot in current magnitude is being reduced with the application of the adaptive droop mechanism, and hence, it improved the stability to a greater extent. Also, the classical droop does not guarantee accurate reactive power sharing among DGs, and hence, virtual output impedance comes out to be an effective approach to tackle this issue [10]. A control method comprising the adaptive virtual impedance-based voltage source inverter (VSI) is designed to enhance the stability and power-sharing performance by modulating the output impedance of the VSI [11]. The aforementioned control strategy is only targeted to enhance the performance of the system by executing some modifications in the classical droop scheme. Moreover, the design mechanism of droop control is considered in such a way that its characteristics rely on the attributes of inverter-based DG such as small inertia, fast dynamic response, better flexibility, and also, the inverter is utilized efficiently if it operates within its generation capability. The peculiarity of classical droop is its inherent delay and hence, the power flow strategy in *P–f*/*Q–E* droop is replaced with the flow of current [12]. The proportion flow of current is established between DG units by employing the *V–I* droop strategy. A suitable droop coefficient enables proportional sharing of power among DGs. Thus, the paper proposed a new methodology for designing the computation method for determining the *V–I* droop coefficient.

The efficiency and conservation of electrical energy are the main concerns for a future microgrid. CVR is the well-known approach to performing demand reduction in the electrical distribution network. CVR involves a voltage reduction mechanism to accomplish energy conservation and consequently, it brings down the losses and peak demand [13]. Moreover, a robust CVR factor formulation is developed by utilizing the soft constrained gradient analysis dependent on time-varying modelling of loads which provides promising results even in case of low time resolution or limited measurements [14]. The voltage source inverter (VSI) plays the lead role in integrating renewable sources of energy with the AC loads. The primary role of VSI is power generation from renewable sources. Apart from its power generating adequacy, the VSI operation involves ancillary utilities such as harmonic reduction, compensation of voltage imbalances, and demand side management [15], [16]. The VSI facilitates demand side management by employing CVR phenomena and generally, there are only two schemes that exist to deduct voltage in grid-connected MG. One technique is termed a no-voltage feedback scheme where line drop compensators and capacitors are used to reduce voltage. Another one is a close loop voltage feedback scheme which utilizes an advanced metering system and SCADA to deduct the voltage parameter [17]. However, the slow response characteristics of voltage-regulating devices are one of the challenges faced by the distribution substation [18]. In addition, the distance between voltage-regulating devices and microgrids could be the reason that drastically affects the CVR execution [19]. A real-time power smoothing control set-up is designed for the distribution network which enables the high penetration of photovoltaic (PV) in coordination with the CVR strategy which smoothens the power fluctuations of the total load caused by the intermittent nature of PV sources [20]. Thus, the execution of CVR for grid-connected microgrids could not fully fulfil the demands such as energy saving with the support of CVR. Hence, this paper proposed the execution of CVR for stand-alone MG with advanced control methodology which characterizes voltage deduction coordinated by *P–f* droop and *V–I* droop strategy.

The attributes of VSI-operated DG in a stand-alone microgrid are the close proximity between load and microgrid and the fast response of VSI would increase the efficiency and range of the CVR mechanism. Recently, a study is being carried out to investigate the potential of CVR for stand-alone MG and its adequacy is realized by comparing the performance with conventional droop [21]. However, the aforementioned study neglected the operational capability limit of the VSI, and only power-saving phenomena are presented with the utilization of CVR. It is very necessary to consider the operational capability limit of VSI and this point must be taken care of while designing the control strategy. Hence, the paper is focused on developing the control mechanism which considers the operational limit of VSI and if the power-delivering capability of VSI goes beyond the limit then CVR action would be carried out. Moreover, the load-shedding control mechanism would get triggered if CVR autonomously would not be able to bring the operational limit of VSI within the predetermined limit. The control methodology is validated through a test system as described in [22]. This paper aims to carry out the following approach:

1. Devised the modified approach to compute the *V–I* droop coefficient.
2. Developed the control methodology to execute the CVR action by coordinated control method involving the operation of *V–I* droop and *P–f* droop control.
3. Designed the control mechanism for load shedding if CVR autonomously is not able to bring the power-delivering capability of VSI under a safe limit.

The remaining section of the paper is outlined as follows: Section 2 states the CVR methodology with a detailed explanation of the droop mechanism. Section 3 discusses the modified version of the droop phenomena to be utilized in the proposed scheme. Section 4 demonstrates the control strategy involving CVR and load shedding mechanism. Section 5 illustrates the validation of the coordinated operation of CVR and load-shedding strategy by analyzing simulation results. Section 6 stipulates the conclusions derived from the work.

2 | CVR APPROACH IN COORDINATION WITH VSI ENABLED DROOP STRATEGY

The CVR mechanism proved to be a convincing technology to minimize the consumption of energy and peak demand. Generally, the CVR mechanism is applied to the upstream end service in the distribution sector to maximize the benefit of increased efficiency by the consumer. The tolerance band of IEEE 1547.2 allows regulation of voltage within 88–110 % and the paper utilized this aforementioned range to perform the CVR scheme. The advantage of CVR execution is the power deduction by the end-user load on reducing the voltage magnitude.

The droop control in the microgrid emerges to be an effective technique to replicate the drooping phenomena in a conventional generator set. The droop control facilitates self-regulation of active and reactive power allocation for the DG, and it is dynamically varying with the change in voltage and frequency magnitude. The *V–I* droop and active power-based *P–f* droop are utilized to control the power. The droop control mode that is responsible for managing frequency is represented as follows:

$$\omega_{fr} = \omega_n - m_k * P_{inv} \tag{1}$$

where ω_n and ω_{fr} depicts the nominal and reference frequency of the DG set. The term P_{inv} represents the active power and m_k is the droop gain used to determine the reference frequency. The voltage $V_{gen,d}$ produced by *V–I* droop control greater than the nominal voltage V_{nom} as it constitutes output current I_{inv} of the inverter multiplying with the droop coefficient Z_l. The *V–I* droop acts as a self-sustained droop that simply performs the function of a resistor. The *V–I* droop is represented as follows [23, 24]: -

$$V_{gen,d} = V_{nom} + Z_l * I_{inv} \tag{2}$$

The droop gains m_k and Z_l of *P–f* and *V–I* droop can be written as follows:

$$m_k = \frac{\omega_n - \omega_{mn}}{P_{inv,\max}}, Z_l = \frac{V_{gen,d} - V_{mn}}{I_{inv,\max}} \tag{3}$$

The allocation of power to the DG is guided by the droop gain m_k and Z_l and hence, it is of utmost importance to choose the suitable value of droop gain to share accurate power among DGs. The minimum voltage and frequency maintained by the controller of the microgrid are represented by V_{mn} and ω_{mn} respectively. The operational capability of the inverter restricts the dispatch of power beyond $P_{inv,\,max}$ corresponding to the output current $I_{inv,\,max}$ respectively to the loads. According to Figure 1, the microgrid's operational frequency is ω_p, which corresponds to the actual power P_i that is produced by the inverter. The *V–I* droop produces a nominal voltage $V_{gen,d-op}$ and it generates a proportional current I_{gd} respectively. As seen from Figure 1, the *V–I* droop encounters voltage rise phenomena with the output current of the inverter and hence, it can be termed a self-sustained droop as it is independent of the microgrid's essential parameters as in the case of conventional power-based droop. The operational capability of the inverter could not exceed beyond $P_{inv,\,max}$ and if this condition occurs then the frequency of the microgrid falls below ω_{mn} which clearly indicates the overloading of the VSI as described in Figure 1. Furthermore, according to the literature in [25], VSI can safely provide 150% of rated current for a duration of 1 min. Hence, the paper proposed a control strategy to shed the non-critical load to safely operate the VSI within its safe limit.

3 | ADAPTIVE VECTOR CONTROL ENABLED VOLTAGE REGULATION

The rotation of the *d–q* reference frame at speed ω_{fr} is utilized to decouple the regulation of active and reactive power by exploiting the benefits of a vector control scheme. The alternating current has a frequency of ω_{fr} produces steady state *d–q* current component i_d and i_q which is the DC component representation in the *d–q* reference frame rotating at a similar speed of ω_{fr}. When the output voltage is positioned along the *d*-axis of the two-axis *d–q* reference frame, the current i_d controls the active power while the current i_q regulates the reactive power. The equation for output voltage can be represented as follows:

$$\begin{bmatrix} V_{fa} \\ V_{fb} \\ V_{fc} \end{bmatrix} = R_f \begin{bmatrix} I_{fa} \\ I_{fb} \\ I_{fc} \end{bmatrix} + L_f \frac{d}{dt} \begin{bmatrix} I_{fa} \\ I_{fb} \\ I_{fc} \end{bmatrix} + \begin{bmatrix} V_{inv,a} \\ V_{inv,b} \\ V_{inv,c} \end{bmatrix} \tag{4}$$

The conversion of an. (4) into a two-axis *d–q* reference frame rotating at a speed ω_{fr} can be written as follows:

$$V_{fd} = R_f I_{fd} + L_f \frac{dI_{fd}}{dt} - \omega_{fr} L_f I_{fq} + V_{inv,d} \tag{5}$$

$$V_{fq} = R_f I_{fq} + L_f \frac{dIq}{dt} + \omega_{fr} L_f I_{fd} + V_{inv,q} \tag{6}$$

where V_{fd} and V_{fq} are voltage generated by the inner loop control. The constant $V_{inv,d}$ and $V_{inv,q}$ are the voltages of the

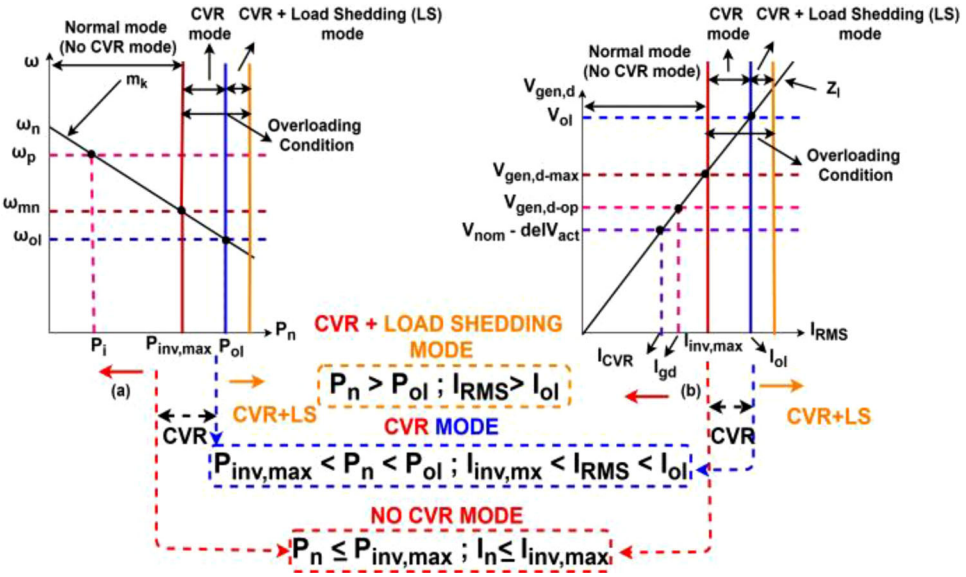

FIGURE 1 Frequency and voltage management scheme.

converter and I_{fd} and I_{fq} represent the current in the two-axis d–q reference frame. The equation representing the active and reactive power can be described as follows:

$$P_{is} = \frac{3}{2}(V_{fd}I_{fd} + V_{fq}I_{fq}) \tag{7}$$

$$Q_{is} = \frac{3}{2}(V_{fq}I_{fd} - V_{fd}I_{fq}) \tag{8}$$

The representation of the angular position θ_{is} in the d–q reference frame can be written as:

$$\theta_{is} = \int \omega_{fr}dt = \tan^{-1}\frac{V_{f\beta}}{V_{f\alpha}} \tag{9}$$

where the term $V_{f\alpha}$ and $V_{f\beta}$ depicts the voltage component of ac source in stationary $\alpha\beta$ axes.

The alignment of the d-axis of the d–q reference frame along the voltage component of the AC source is depicted in Eq. (9) and the positioning of the vector component of the voltage and current can be represented as shown in Figure 2 which shows the voltage component $V_{fq} \approx 0$ and the voltage V_{fd} tends to be equal to the magnitude of the AC voltage V_f. Hence, it can be summarized that the exchange of active and reactive power between the AC source and converter is equivalent to the current the regulation of active and reactive power can be achieved by controlling the current component I_{fd} and $I_{fq}$and further, the Hence, the expression for power can be depicted as follows:

$$P_{is} = \frac{3}{2}V_{fd}I_{fd} \tag{10}$$

$$Q_{is} = -\frac{3}{2}V_{fd}I_{fq} \tag{11}$$

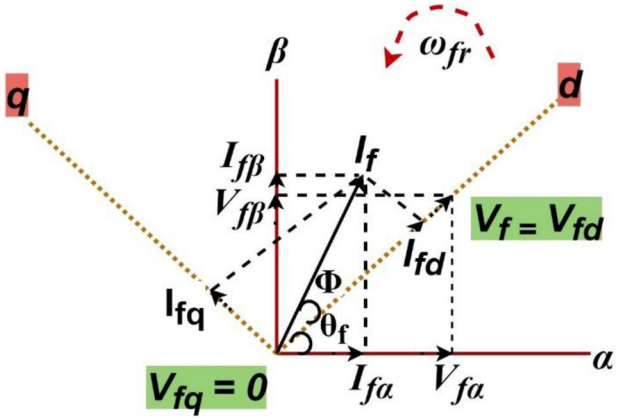

FIGURE 2 Representation of voltage-oriented vector control of AC voltage on two-phase d–q reference frame.

4 | DROOP CONTROL SCHEME

This section illustrates the classical and modified droop estimation method and the final matrix tends to produce a droop coefficient for V–I droop determined by taking into account a network made up of 3 buses and 5 impedances. The detailed method is explained in the consecutive section.

4.1 | Classical V–I droop estimation method

The droop gain Z_l needs to be determined to achieve accurate sharing of power among DGs. The procedure to compute the V–I droop gain considered the summation of individual nodes present in the network with the other node to represent the impedance between these two nodes. Similarly, the method covers all the branches of the impedances in the network, and it

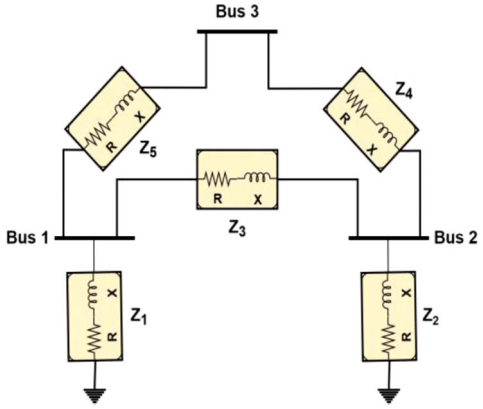

FIGURE 3 Representation of network comprising 3 bus with 5 impedance.

is important to note that the branch connection between two nodes produces a matrix whose size is determined by the number of nodes. Subsequently, the matrix size would increase with the inclusion of new nodes to connect each of the impedances present in the network.

For defining the procedure, a 5-bus network that includes 3 nodes and 5 impedances shown in Figure 3 is considered to show the detailed method in a lucid way. As there are 3 nodes present in the network, hence, the size of the matrix at the final stage would be 3 × 3 and the detailed representation of droop computation for V-I droop is shown in Figure 4 and discussed in the subsequent section.

4.2 | Modified estimation of *V–I* droop coefficient

The formation of Z_{dr} matrix is carried out in the following steps:

Step 1: The interconnection of Z_1 is joined from point V_1 to reference point J and it leads to the initiation of the current I_1. The expression is written as follows:

$$V_1 = Z_1 * I_1 \tag{12}$$

and the matrix representation of the above expression is:

$$Z_{dr} = [Z_1] \tag{13}$$

Step 2: Further, the line impedance Z_2 is interconnected between point V_2 and reference point J. The resultant expression turns into a matrix as follows:

$$V_{dr} = \begin{bmatrix} V_1 \\ V_2 \end{bmatrix} = \begin{bmatrix} Z_1 & 0 \\ 0 & Z_2 \end{bmatrix} \begin{bmatrix} I_1 \\ I_2 \end{bmatrix} \tag{14}$$

Also, $Z_{dr,OLD} = [Z_1]$

The resultant matrix for $Z_{dr,NEW}$ would be represented as follows:

$$Z_{dr,NEW} = \begin{bmatrix} Z_{dr,old} & 0 \\ 0 & Z_2 \end{bmatrix} \tag{15}$$

where $Z_{dr,OLD} = [Z_1]$.

Step 3: The integration of new impedance Z_4 between point 2 and point 3 leads to the following matrix as follows:

$$\begin{bmatrix} V_1 \\ V_2 \end{bmatrix} = \begin{bmatrix} Z_1 & 0 \\ 0 & Z_2 \end{bmatrix} \begin{bmatrix} I_1 \\ I_2 + I_3 \end{bmatrix} \tag{16}$$

$$V_3 = V_2 + Z_4 I_3 \tag{17}$$

$$\begin{bmatrix} V_1 \\ V_2 \\ V_3 \end{bmatrix} = \begin{bmatrix} Z_1 & 0 & 0 \\ 0 & Z_2 & Z_2 \\ 0 & Z_2 & Z_2 + Z_4 \end{bmatrix} \begin{bmatrix} I_1 \\ I_2 \\ I_3 \end{bmatrix} \tag{18}$$

Now, the transformed $Z_{dr,NEW}$ the matrix can be written as follows:

$$\begin{bmatrix} & & & Z_{1J} \\ & Z_{bus,OLD} & & Z_{2J} \\ & & & \vdots \\ & & & Z_{KJ} \\ Z_{J1} & Z_{J2} & \cdots & Z_{JK} \quad Z_{JJ} + Z_{NEW} \end{bmatrix} \tag{19}$$

Step 4: The point 1 and point 2 connect line impedance Z_3 leads to the flow of current i_L in the loop 12J and the current at point 1 and point 2 is $+i_L$ and $-i_L$ respectively. The resultant expression is as follows:

$$\begin{bmatrix} V_1 \\ V_2 \\ V_3 \end{bmatrix} \begin{bmatrix} Z_{11} & Z_{12} & Z_{13} \\ Z_{21} & Z_{22} & Z_{23} \\ Z_{31} & Z_{32} & Z_{33} \end{bmatrix} \begin{bmatrix} I_1 + i_L \\ I_2 - i_L \\ I_3 \end{bmatrix} \tag{20}$$

The size of the formulated matrix is considered to be $P \times P$ and the integration of any new line impedance Z_{new} between the point, 'g' and point 'h' comprising 'P' number of nodes results in the matrix with the loop current i_L as follows:

$$\begin{bmatrix} V_1 \\ V_2 \\ \vdots \\ V_g \\ V_h \\ \vdots \\ V_{P-1} \\ V_P \end{bmatrix} = \begin{bmatrix} Z_{1,1} & Z_{1,2} & \cdots & \cdots & \cdots & Z_{1,P-1} & Z_{1,P} \\ Z_{2,1} & Z_{2,2} & \cdots & \cdots & \cdots & Z_{2,P-1} & Z_{2,P} \\ \vdots & \vdots & \cdots & \cdots & \cdots & \vdots & \vdots \\ Z_{g,1} & Z_{g,2} & \cdots & \cdots & \cdots & Z_{g,P-1} & Z_{g,P} \\ Z_{h,1} & Z_{h,2} & \cdots & \cdots & \cdots & Z_{h,P-1} & Z_{h,P} \\ \vdots & \vdots & \cdots & \cdots & \cdots & \vdots & \vdots \\ Z_{P-1,1} & Z_{P-1,2} & \cdots & \cdots & \cdots & Z_{P-1,P-1} & Z_{m-1,m} \\ Z_{P,1} & Z_{P,2} & \cdots & \cdots & \cdots & Z_{P,P-1} & Z_{P,P} \end{bmatrix} \begin{bmatrix} I_1 \\ I_2 \\ \vdots \\ I_g + i_L \\ I_h - i_L \\ \vdots \\ I_{P-1} \\ I_P \end{bmatrix} \tag{21}$$

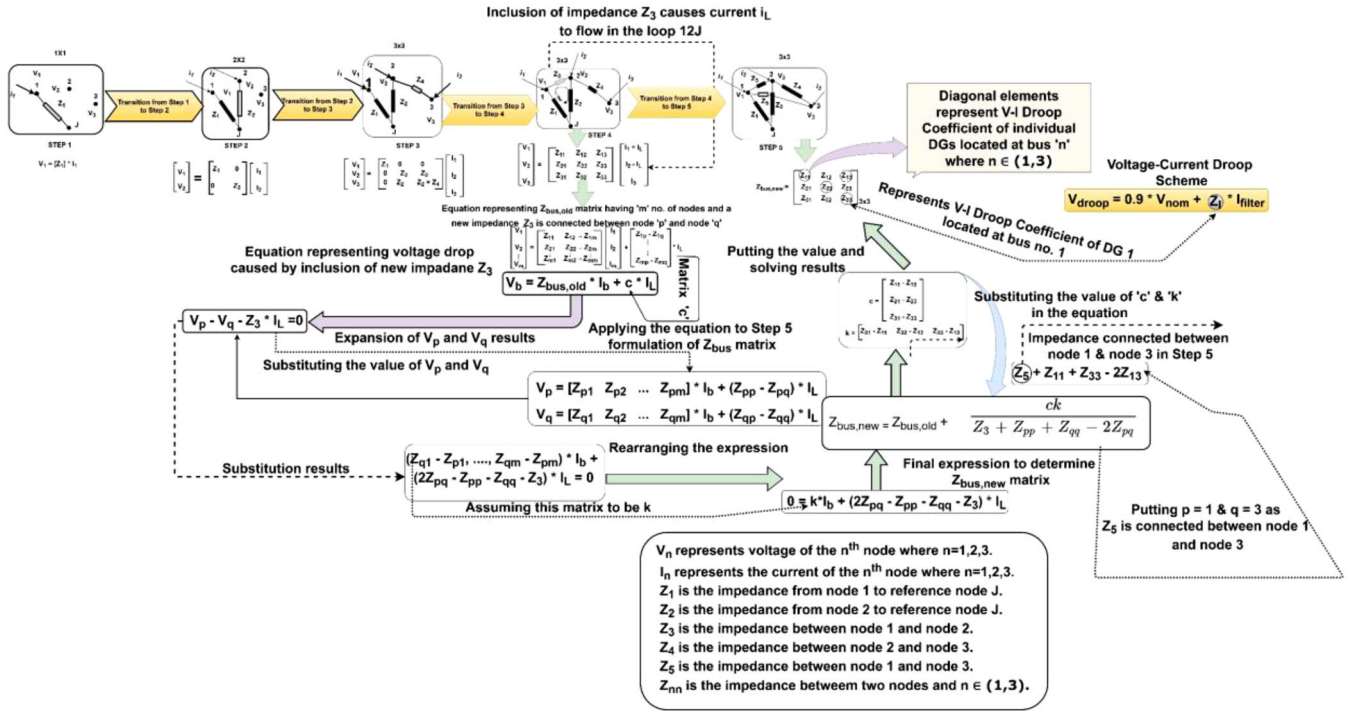

FIGURE 4 Computation mechanism for V–I droop coefficient.

Further, the Eq. (21) can be modified to the following matrix:

$$\begin{bmatrix} V_1 \\ V_2 \\ \vdots \\ V_P \end{bmatrix} = \begin{bmatrix} Z_{1,1} & Z_{1,2} & \cdots & Z_{1,P} \\ Z_{2,1} & Z_{2,2} & \ldots & Z_{2,P} \\ \vdots & \vdots & \ddots & \vdots \\ Z_{P,1} & Z_{P,2} & \cdots & Z_{P,P} \end{bmatrix} \begin{bmatrix} I_a \\ I_b \\ \vdots \\ I_P \end{bmatrix} + \begin{bmatrix} Z_{1g} - Z_{1b} \\ \vdots \\ Z_{Pg} - Z_{Pb} \end{bmatrix} . I_L \quad (22)$$

Again, the Eq. (22) is modified as:

$$V_{bus} = Z_{bus,OLD}.I_{bus} + \mathrm{c}.i_L \text{ where c} = \begin{bmatrix} Z_{1g} - Z_{1b} \\ \vdots \\ Z_{Px} - Z_{Pq} \end{bmatrix} \quad (23)$$

The difference between columns #g and #b is defined by the term 'c' and the $Z_{dr,OLD}$ matrix can be determined as follows:

The voltage drop caused due to integration of impedance Z_3 and it is written as follows:

$$V_b - -V_g = Z_3.i_L \quad (24)$$

$$V_g - V_b - -Z_3.i_L = 0 \quad (25)$$

The expansion of the term V_g and V_b results into the following expression:

$$V_g = \left[Z_{g1}\ Z_{g2}\ \ldots\ Z_{gP} \right] .\ I_{bus} + \left(Z_{gg} - Z_{gs} \right) . i_L \quad (26)$$

And

$$V_b = \left[Z_{b1}\ Z_{b2}\ \ldots\ Z_{bP} \right] . I_{bus} + (Z_{br} - Z_{bb}) . i_L \quad (27)$$

Substituting Eqs. (26) and (27) in Eq. (25) results:

$$\left(Z_{b1} - Z_{g1}\ , \ldots , Z_{bP} - Z_{gP} \right) . I_{bus} + \left(2Z_{gb} - Z_{gg} - Z_{bb} - Z_3 \right) . i_L = 0 \quad (28)$$

The Eq. (28) can be written as follows:

$$0 = \mathrm{y} * I_{bus} + \left(2Z_{gb} - Z_{gg} - Z_{bb} - Z_3 \right) . i_L \quad (29)$$

The row matrix 'y' of N dimensional size is depicted as follows:

$$\mathrm{y} = \left(Z_{b1} - Z_{g1}\ , \ldots , Z_{bP} - Z_{gP} \right) \quad (30)$$

The determination of the loop current i_L is found by solving Eq. (29) and the voltage V_{bus} is illustrated as follows:

$$V_{bus} = Z_{dr,OLD} + \frac{1}{Z_3 + Z_{gg} + Z_{bb} - 2Z_{gb}} . (\mathrm{c} * \mathrm{y} * I_{bus} \quad (31)$$

Further, the Eq. (31) is written as:

$$V_{bus} = \left\{ Z_{dr,OLD} + \frac{\mathrm{c} * \mathrm{y}}{Z_3 + Z_{gg} + Z_{bb} - 2Z_{gb}} \right\} . (I_{bus}) \quad (32)$$

And the voltage $V_{bus} = Z_{dr,NEW} . I_{bus}$ (33)

The resultant expression for $Z_{dr,NEW}$ matrix can be described as follows:

$$Z_{dr,NEW} = Z_{dr,OLD} + \frac{\mathrm{c} * \mathrm{y}}{Z_3 + Z_{gg} + Z_{hh} - 2Z_{gh}} \tag{34}$$

The determined final $Z_{dr,NEW}$ matrix represents the impedance Z_3 coupling between the points #g and #h which actually represents point 1 and point 2 in Figure 4.

Step 5: Finally, the impedance Z_5 is connected between point 1 and point 3 and it is described as:

$$Z_{dr,NEW} = Z_{dr,OLD} + \frac{\mathrm{c} * \mathrm{y}}{Z_5 + Z_{11} + Z_{33} - 2Z_{13}} \tag{35}$$

The resultant final $Z_{dr,NEW}$ matrix can be represented as follows:

$$Z_{dr,NEW} = \begin{bmatrix} Z_{11} & Z_{12} & Z_{13} \\ Z_{21} & Z_{22} & Z_{23} \\ Z_{31} & Z_{32} & Z_{33} \end{bmatrix} \tag{36}$$

The droop coefficient estimation for the V–I droop is computed by knowing the location of the DG. For illustration, Z_{33} element in the $Z_{dr,NEW}$ matrix is the V–I droop coefficient for the DG at bus number 3 and in this way, the droop coefficient computation is easily determined for single-feeder and multi-feeder networks comprising multiple DGs.

4.3 | Coordination of *P–f* droop and *V–I* droop to execute CVR scheme

The CVR mechanism is applied with the coordination of the modified P–f droop strategy and V–I droop strategy. The expression for active power and output current generated by the voltage source inverter during overloading condition is written as follows:

$$P_{ol} = \frac{\omega_n - \omega_{ol}}{m_k}, I_{ol} = \frac{V_{gen,d} - V_{ol}}{Z_l} \tag{37}$$

The term P_{ol} and I_{ol} describes the active power dispatch and output current generated by the inverter during overloading conditions. The three-phase term I_{ol} is transformed into the d–q frame and complex power is described as follows:

$$S_j = \frac{3}{2} V_{gen,d}(I_{d,ol} - jI_{q,ol}) = \frac{3}{2}(V_{gen,d} I_{d,ol} - jV_{gen,d} I_{q,ol}) \tag{38}$$

The expression for reactive power can be derived from Eq. (38) as follows:

$$Q_{ol} = -\frac{3}{2} V_{gen,d} I_{q,ol} \tag{39}$$

Hence, the q axis of the d–q frame provides the reactive power as outlined in Eq. (39). The variation of frequency and voltage parameters would be observed once the microgrid reaches the overloading condition. The imbalance that occurs in the power-sharing mechanism due to the aforementioned variation of parameters can be written as follows:

$$P_{del} = P_{ol} - P_{inv,\max} = \frac{\omega_{\mathrm{m}n} - \omega_{ol}}{m_k} \tag{40}$$

$$Q_{del} = I_{ol} - I_{inv,\max} = \frac{V_{gen,d-\mathrm{mx}} - V_{ol}}{Z_l} \tag{41}$$

The active power P_{del} and reactive power Q_{del} are provided by the inverter during the arrival of overloading conditions. The paper proposed the initiation of the CVR mechanism at the time of peak demand and overloading condition of the stand-alone microgrid. The following equation characterized the normal and CVR mode of the microgrid and it can be expressed as follows:

$$P_{del} = \begin{cases} \dfrac{\omega_n - \omega_{ol}}{m_k} & for\ \omega < \omega_{\mathrm{mn}} \\ 0 & for\ \omega \geq \omega_{\mathrm{mn}} \end{cases} \tag{42}$$

$$I_{del} = \begin{cases} \dfrac{V_{gen,d} - V_{ol}}{Z_l} & for\ V > V_{gen,d-\max} \\ 0 & for\ V \leq V_{gen,d-\max} \end{cases} \tag{43}$$

Hence, the microgrid needs to be maintained the minimum value of frequency ω_{mn} to sustain the normal operating mode. Also, it is important to consider the voltage $V_{gen,d-\max}$ which is proportional to current $I_{d-\max}$ should be within the limit of the voltage source inverter. If any of the limits cross the threshold, then the microgrid reaches the situation of peak demand and overloading mode. The expression for apparent power during overloading mode can be described as:

$$S_{del} = \sqrt{P_{del}^2 + Q_{del}^2} \tag{44}$$

The execution of CVR during peak demand and overloading conditions deducts a specific amount of voltage from every DG connected to the microgrid. Hence, there is a need to establish the relationship between apparent power and output voltage. The static load model is characterized as follows:

$$P_{dm} = P_{ar}\left(\frac{V_{act}}{V_r}\right)^s \tag{45}$$

$$Q_{dm} = Q_{ar}\left(\frac{V_{act}}{V_r}\right)^t \tag{46}$$

The term $P_{dm,}$ and Q_{dm} depicts active and reactive power at the actual voltage V_{act} respectively. At rated voltage V_r, the term P_{dm} *and* Q_{dm} represent active and reactive power. The active and reactive power consumption varies on changing the load voltage from V_r to V_{act} respectively. The s and t are exponential constants that rely on the load characteristic. Let exponential constant $s = t = w$ then the relation between apparent power and voltage is represented as follows:

$$S_j = S_m\left(\frac{V_{act}}{V_r}\right)^w \tag{47}$$

The expression in Eq. (47) depicts the load modelling in per unit and further, the derivative of S_j with respect to V_{act} is found out and it is described as follows:

$$\frac{dS_j}{dV_{act}} = wV_{act}^{w-1} \tag{48}$$

The constant w determines the load constituents, that is, the type of load connected to the microgrid. The value of $w = 2$ represents constant impedance load as CVR would be more pronounced in these types of loads. In other words, the Eq. (48) can be written as follows:

$$delV_{act} = 0.5\frac{delS_j}{V_{gen,d}} \tag{49}$$

The load characteristic constant w is inversely related to the compensation voltage $delV_{act}$ and hence, it can be concluded that with the decreasing value of w, the compensation voltage would increase, that is, w = 1 represents constant current load which needs higher voltage compensation compared to constant impedance load to achieve a similar reduction of power consumption. The output voltage $V_{gen,d}$ is considered to be aligned along the direct axis and hence, the operation of the controller is to ensure that $V_q \approx 0$ respectively. The d-axis voltage $V_{gen,d}$ is utilized to perform the CVR function and it should be noted that the compensation voltage $delV_{act}$ generated by the CVR scheme does not exactly reduce from each of the DG as V–I droop control develops voltage which goes on increasing with the step increase of the load. Therefore, the output voltage provided by the V–I droop control can be modified as follows:

$$V^*_{gen,d} = V_n + I_{inv} * Z_l - delV'_{act} \tag{50}$$

$$delI = \frac{V_{d,mn} - V_{ol} - delV'_{act}}{Z_l} \tag{51}$$

Hence, the expression in Eq. (50) represents the modified equation for V–I droop control that provides output voltage by the inverter in case of CVR execution.

5 | EXECUTION OF THE PROPOSED CONTROL SCHEME

5.1 | Proposed CVR scheme

Figure 5 depicts the normal, CVR, and overloading mode of the standalone microgrid. The operating active power and output current of the inverter stays within $P_{inv,\max}$ *or* $I_{inv,\max}$ then it characterized the normal condition of the microgrid. The CVR mechanism is not functional during this condition and hence, $delV_{act} = 0$. The normal mode is represented as follows:

$$P_n \le P_{inv,\max}, I_n \le I_{inv,\max} \tag{52}$$

The load demand beyond the operating capability of the VSI would trigger the CVR control mechanism and further, a compensating voltage is provided by the CVR scheme. The generation of compensating voltage depends upon the value of ω_{mn} and $V_{gen,d-mx}$ respectively. The sample and hold circuit of the CVR mechanism produces $delV_{act}$ on reaching the region as described by Eq. (53) and it results in a reduction of voltage from each of the DG units to reduce the power consumption. The aforementioned operation brings the operation of the microgrid back to normal mode as characterized by Eq. (52) and different operating modes are clearly depicted in Figure 5. The equation representing CVR mode is as follows:

$$P_{inv,\max} < P_n < P_{ol}, I_{inv,\max} < I_n < I_{ol} \tag{53}$$

5.2 | Execution of control strategy during overloading condition

The load shedding strategy comes into action once the operation of the microgrid falls beyond the region of the CVR scheme, that is, P_{ol} and I_{ol} and it reaches the region of overloading condition as represented in Figure 5. The magnitude of load reduction is decided by the following expression:

$$P_{ls} = \sum_{r=1}^{t}\frac{1}{m_{kr}}(\omega_{\mathrm{mn}} - \omega_{mr})S_{cr} \tag{54}$$

$$Q_{ls} = \sum_{r=1}^{t}\frac{1}{Z_{lr}}(V_{gen,d,\mathrm{mn}} - V_{ol,r} - delV_{act})S_{cr} \tag{55}$$

The droop gain for the rth VSI is represented by the terms m_{kr} and Z_{lr} respectively. The apparent power S_{cr} depicts the rating of the rth inverter. After the execution of the CVR strategy, the frequency and voltage would become ω_{mr} and $V_{ol,r}$ respectively. The constant t exhibits the total number of inverters operating in the microgrid. The enabling of load shedding strategy on exceeding the P_{ol} and I_{ol} is the clear indication of load reduction and hence, load shedding control scheme determines P_{ls} and Q_{ls} which provides the amount of non-critical load disconnected from the microgrid.

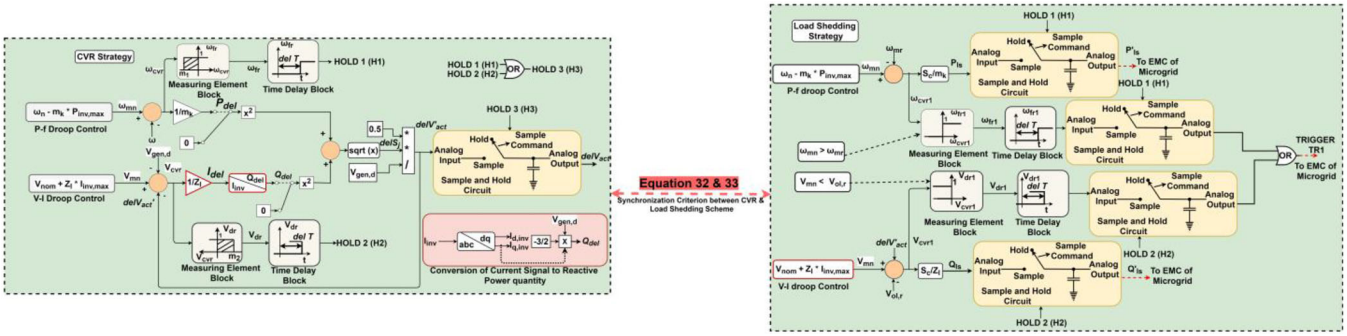

FIGURE 5 Representing CVR and load shedding scheme.

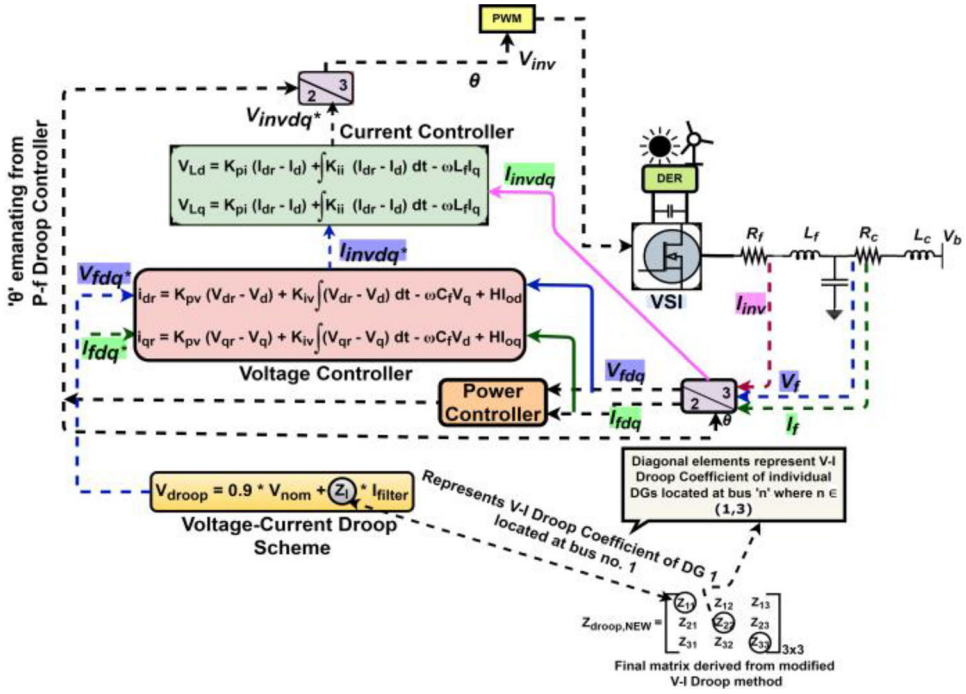

FIGURE 6 Cascade control scheme.

5.3 | Establishing control coordination between load shedding strategy and CVR scheme

The synchronous operation of CVR and load shedding mechanism is required when CVR is unable to bring the capability of the inverter shown in Figure 5 within its range and the cascade control mechanism is represented in Figure 6. Figure 7 illustrate the operational flow chart of MG. The constants $\mathbf{m}_1$ and $\mathbf{m}_2$ in the measuring element of *P–f* and *V–I* droop are considered very small and the value of $\mathbf{m}_1 = -0.0006$ pu and $\mathbf{m}_2 = +0.0006$ pu.

$$m_1 \leq \omega_{cvr} \leq 0, 0 \leq V_{cvr} \leq m_2 \tag{56}$$

The triggering of load shedding strategy enables the calculation of active and reactive power to be curtailed from the microgrid as described by Eqs. (54) and (55). The operational parameters of the controller are described in Table 1 and the modes of operation of MG are described in Table 2. The parameters of measuring element to conduct synchronous operation of CVR and load shedding scheme is set as follows:

$$\omega_{fr}, V_{dr} = \begin{cases} \text{False for } \omega_{cvr} < m_1, V_{cvr} > m_2 \\ \text{True for } \omega_{cvr} \geq m_1, V_{cvr} \leq m_2 \end{cases} \tag{57}$$

$$\omega_{fr1}, V_{dr1} = \begin{cases} \text{False } for\ \omega_{cvr1} \leq 0,\ V_{cvr1} \geq 0 \\ \text{True } for\ \omega_{cvr1} > 0,\ V_{cvr1} < 0 \end{cases} \tag{58}$$

6 | SIMULATION VALIDATION OF THE PROPOSED SCHEME

The validation of the proposed CVR and load shedding scheme is carried out through microgrid test bed shown in Figure 8. This section comprises of two case studies and it is illustrating

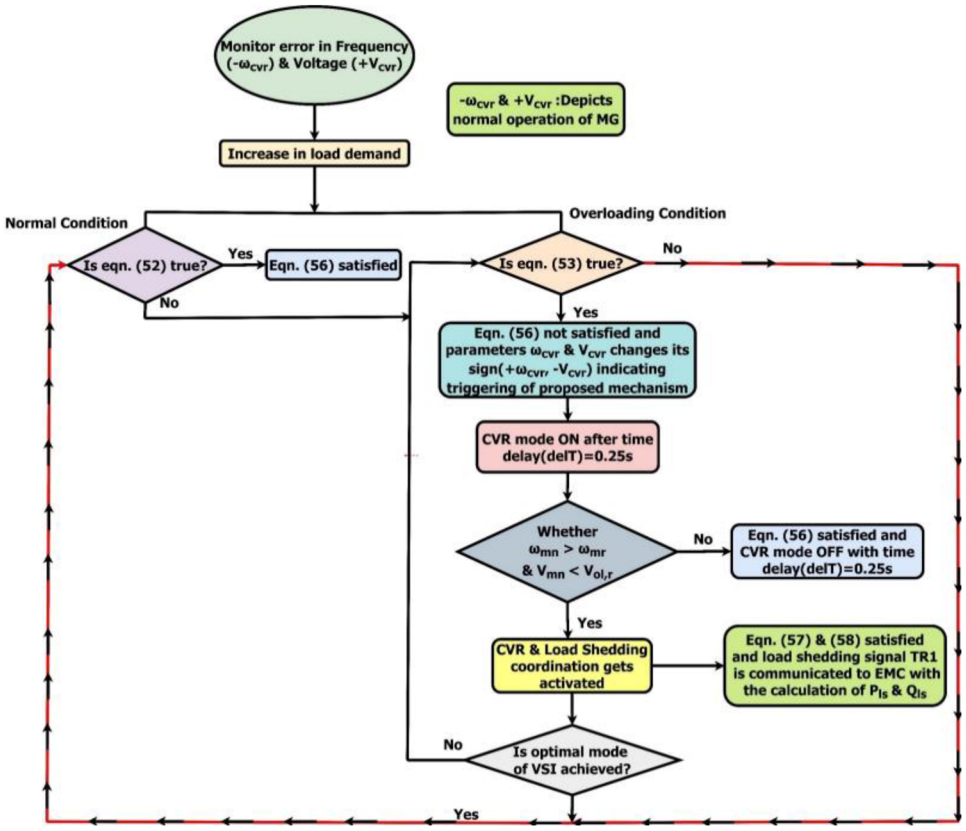

FIGURE 7 Flow chart representing operation of MG.

TABLE 1 Specifications of MG

DG's specification	
Droop gains in the *P–f*/*V–I* droop	$m_k = 0.02$ pu (Peak demand condition);$m_{k1} = = 0.04$ pu, $m_{k2} = 0.01$ pu (Overloading Condition).$Z_{l1} = 0.0178\ \Omega$, $Z_{l2} = 0.022\ \Omega$, $Z_{l3} = 0.206\ \Omega$
Parameters for outer voltage loop	$K_{pv} = 5$; $K_{iv} = 257$
Parameters for inner current loop	$K_{pi} = 11$; $K_{ii} = 1800$
Filter's specification	$L_{fil} = 0.5$ mH, $C_{fil} = 70\ \mu$F, $R_{fil} = 0.15\ \Omega$

TABLE 2 Modes of operation of MG

Modes	Signs	Controller's response
CVR OFF	$-\omega_{cvr}$ & $+V_{cvr}$	$delV_{act} = 0$, H3 = 0
CVR ON	$+\omega_{cvr}$ & $-V_{cvr}$ and $\omega_{mn} < \omega$ & $V_{mn} > V_{gen,d}$	$delV_{act} = 1$, H3 = 1
CVR+Load shedding	$\omega_{mn} > \omega_{mr}$ & $V_{mn} < V_{ol,r}$	$delV_{act} = 1$, H3 = 1 & calculation of P_{ls} and Q_{ls}

the coordination of *P–f* droop and *V–I* droop to perform the CVR scheme and load shedding mechanism.

6.1 | Performance evaluation in case of peak demand condition

The application of CVR in the case of peak demand conditions is demonstrated for the microgrid network shown in Figure 8. The effectiveness of the proposed scheme is shown by comparing the result in CVR ON and OFF modes. In this test scenario, the concept of overloading is not discussed, and hence, the activation of synchronous operation of CVR and load shedding strategy is not necessary. For this test condition, it is considered that the CVR strategy gets activated if the active and reactive power reaches the threshold value of 80% of peak demand operating at 0.95 pf to preserve consumption of energy. The evaluation of the result is scaled down to a 2 s time frame to clearly observe the performance of the CVR mechanism in case of a peak demand situation.

The loading of the microgrid between the time interval 0–1 s represents the operation of the microgrid below the 80% limit. The parameters of the microgrid are demonstrated in Figures 9–13. During the time interval of 0–1 s, the active and reactive power shown in Figure 9 which exhibit the microgrid's operation below the 80% limit. The frequency variation of the microgrid is shown in Figure 10. Figure 11 exhibits the active and reactive power output provided by the individual DG. The sharing proportion of active power of the DG is decided by the droop gain ***mp*** set in the *P–f* droop and droop coefficient ***Zk*** in the *V–I* droop scheme. The voltage at the PCC terminal is

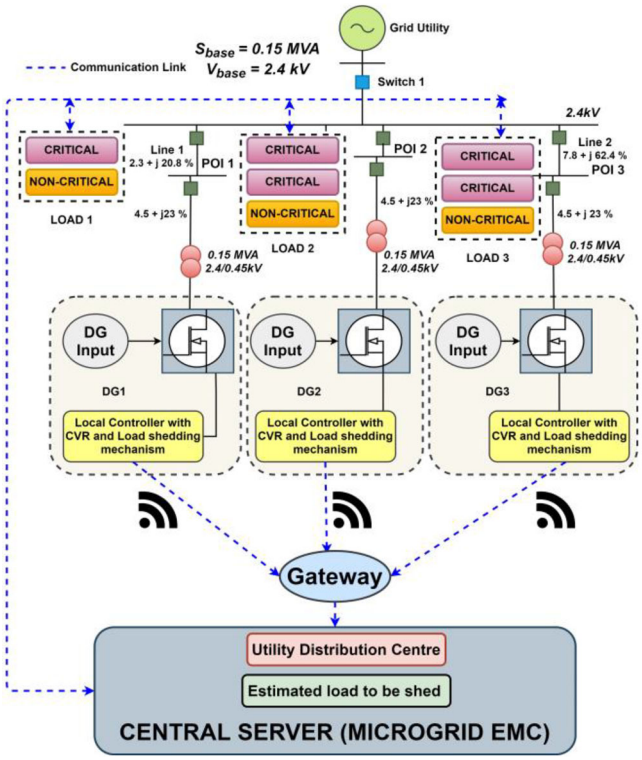

FIGURE 8 Microgrid test bed.

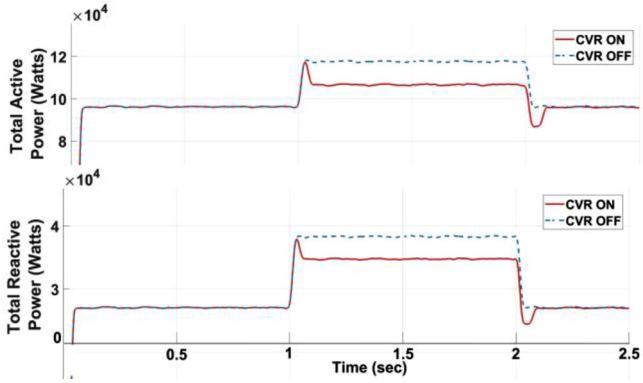

FIGURE 9 Total power of microgrid.

demonstrated in Figure 12 and it is clearly seen that the voltage band is within the acceptable limit as described in Section 4. As seen in Figure 13, the voltage compensation *delV* during the time interval is 0–1 s is 0 as CVR is not being triggered during this aforementioned loading condition.

The loading condition of MG is increased by 22.36 kVA at time $t = 1$s to exceed the demand of VSI beyond 80% to demonstrate the CVR mechanism during peak demand conditions. The aforementioned condition activated the CVR mechanism which is identified in Figure 9, and it depicts the overall active and reactive power scenario during peak demand operation. The frequency parameter is shown in Figure 10 which shows improvement with the application of the CVR strategy. The peak demand condition affects the frequency and voltage parameter and subsequently, the measuring element realizes this change to trigger the CVR mechanism. The proposed CVR methodology is depicted in Figure 5. With the abrupt change in the frequency or voltage parameter tends to determine the compensating voltage *delV* which got subtracted from the voltage controller reference *d*-axis to perform CVR action. Subsequently, the DGs would experience the lowering of voltage as demonstrated in Figure 12. The voltage developed at the PCC function in the lower range of voltage which would lower the power consumption of load elements. Consequently, the microgrid's consumption of power reduces with the application of the CVR scheme as depicted in Figure 11. The dashed line in Figures 9–13 depicts the OFF mode of CVR. As it is clearly evident from Figures 9–12, the power output during the OFF mode of CVR is higher as compared to the ON duration of CVR. The voltage compensation scheme is clearly visible in Figure 13 which is calculated on the basis of changes in frequency and voltage parameters. During times of peak demand, the proposed CVR scheme preserves power in the range of 11−16%. Finally, the off-peak demand situation occurs at $t = 2$ s by disconnecting the load from PCC 1 which brings back the operation of the microgrid as depicted during the time interval of $t = 0$–1 s.

6.2 | Performance evaluation of control coordination between CVR and overloading condition

This case study demonstrates how CVR and load shedding works together to address the overloading issue of the microgrid. Figures 14–20 depicts the transition of the microgrid's parameter from overloading mode to normal mode. The operational scenario of a microgrid at time $t < 0.6$ s represents the normal zone. The net demand of active and reactive power is represented in Figure 14. The power-sharing proportion among DGs is shown in Figures 15 and 16 and it is dependent on the droop gains of the *P*–*f* and *V*–*I* droop.

The time interval $t < 0.6$ s represents non-activation of the CVR mechanism which produces the value of compensating voltage $\mathbf{delV}_{\mathbf{act}} = 0$ as shown in Figure 17. It is well known that constant impedance load is more sensitive to voltage variation, hence, the circuit breaker connects 10.8 kVA of constant impedance load at $t = 0.6$ s. The abrupt load demand disturbs the microgrid's voltage and frequency parameter and the triggering of the CVR mechanism is observed on reaching the preset limit in the measuring element of the control scheme shown in Figure 17. The power output and frequency variation on actuating CVR mechanism is clearly observed in Figures 14 and 18. The time delay ($t = 0.25$ s) is provided to the compensating voltage $\mathbf{delV}_{\mathbf{act}}$ through signal Hold 3 to ensure its steady state operation and so, the CVR would remain ON during this time period. The overloading mode of operation of DG is clearly observed in Figure 19 which reduces the voltage at the PCC. The output current of DG 1 at $t = 0.6$ s marginally touched the 1 pu limit and hence, it tends to activate the CVR strategy. Consequently, the power consumption would get reduced

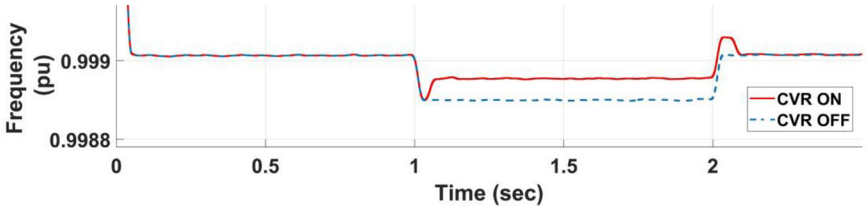

FIGURE 10 Frequency during peak demand operation.

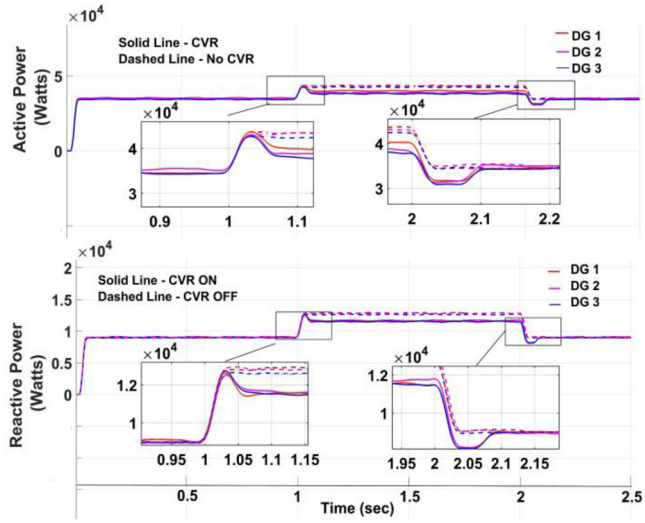

FIGURE 11 Scenario of active and reactive power during peak demand operation.

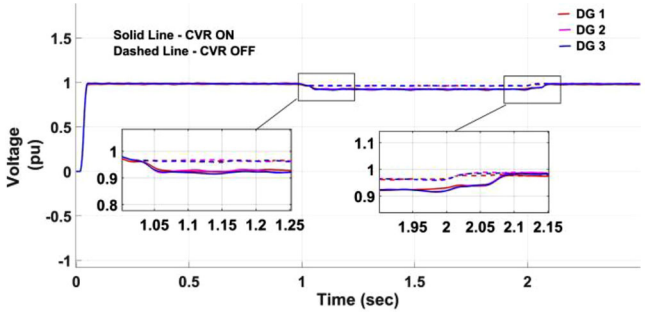

FIGURE 12 Representing voltage of three DG in pu.

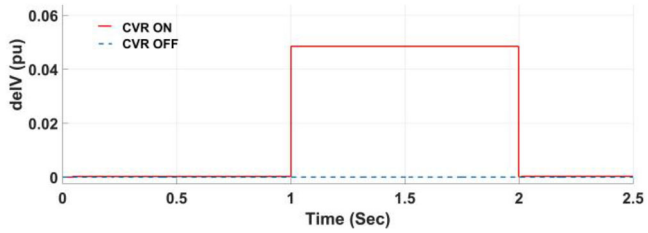

FIGURE 13 Voltage compensation during peak demand operation.

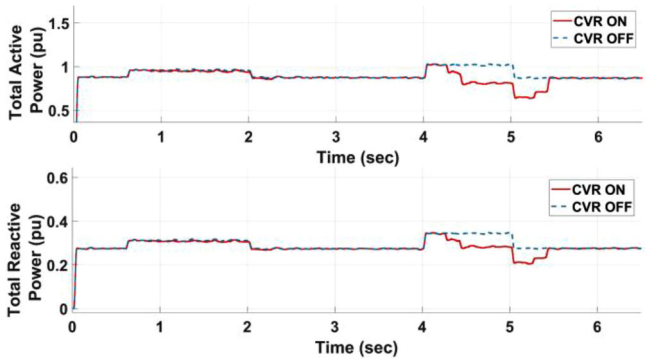

FIGURE 14 Total active and reactive power variation during overloading situation.

as shown in Figures 15 and 16 once voltage deduction signals are provided by the CVR mechanism. Due to the direct relationship between voltage $\mathbf{delV_{act}}$ and apparent power $\mathbf{S_j}$, a very small voltage deduction signal is provided by the CVR strategy at $t = 0.6$ s and hence, there is a very small reduction in total power consumption (0.006 pu) as shown in Figure 14. Moreover, the load shedding strategy is deactivated during this time period as the current of all the DGs is within the specified limit (1 pu).

The result shown in Figure 14 ensures that during the CVR phenomena, the reduction in the total power is achieved in comparison to the control strategy without CVR. The non-critical load required to be shed in case of control strategy without CVR as Figures 14 and 20 shows DG1 is in overloaded condition by a very small amount. The circuit breaker disconnects the additional load at time $t = 2$ s and the operational parameter of the microgrid settled to the preceding state as exhibited before time $t < 0.6$ s. The H3 signal provides a time delay of 0.25 s to the CVR mechanism and deactivation of CVR is ensured after time $t = 2.25$ s as shown in Figure 17. At PCC2, the circuit breaker connects a constant impedance load of 41.3 kVA at time $t = 4$ s. This result sudden increase of power of DG 2 which energizes the CVR strategy as frequency tends to become positive and voltage changes its state to negative as set in the measuring block shown in Figure 5. Figures 14 and 20 depict the overloading condition of DG for a brief time of 0.25 s and consequently, the CVR get activated at $t = 4.25$ s to produce compensating voltage $delV_{act}$ as shown in Figure 17. Moreover, a large change in load causes the PCC voltage to reduce as depicted in Figure 19 and this curtails the power consumption of the microgrid. However, on observing the performance of the CVR strategy at time $t = 4.25$ s, the power consumption deduction due to CVR phenomena is not enough to attain the normal operation of the microgrid, and hence, shedding of load required with the enabling of load shedding strategy as stated in (54) and (55). The enabling of load shedding strategy

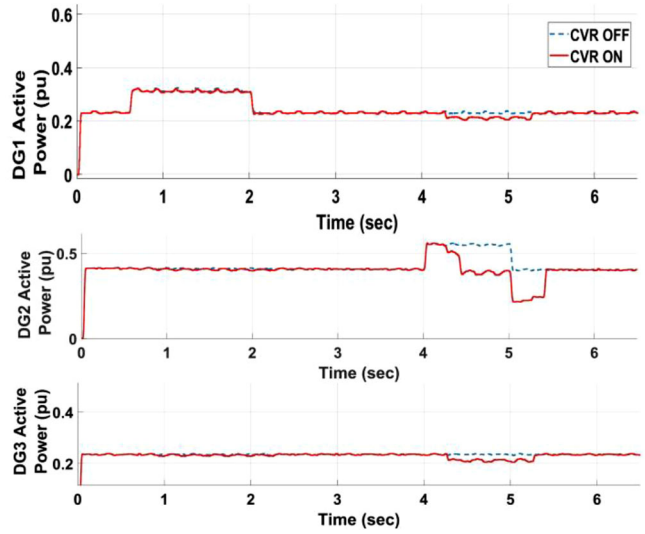

FIGURE 15 Active power variation of DG during overloading situation.

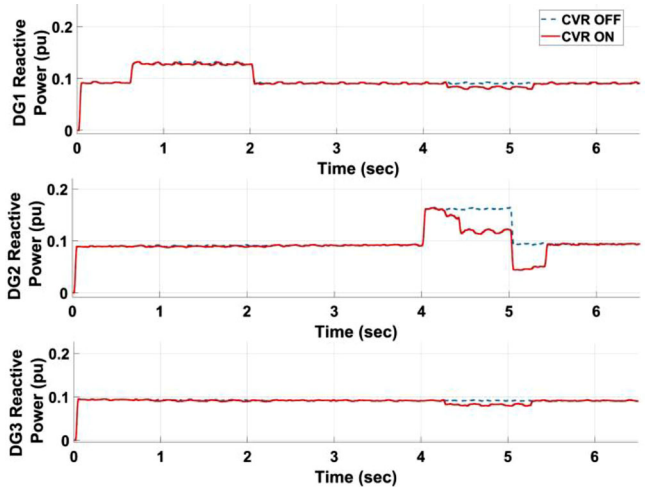

FIGURE 16 Reactive power variation of DG during overloading situation.

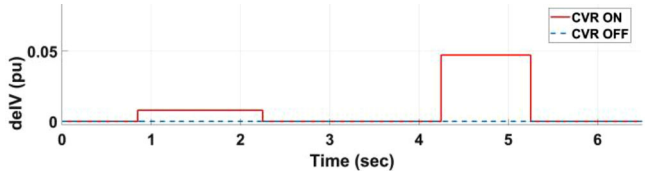

FIGURE 17 Depicting voltage compensation of DG's.

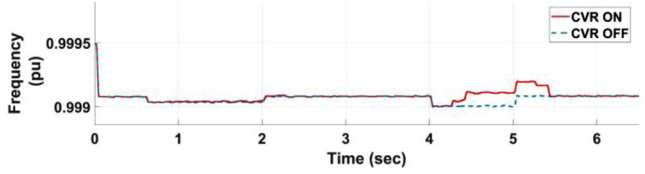

FIGURE 18 Frequency variation during operation of microgrid.

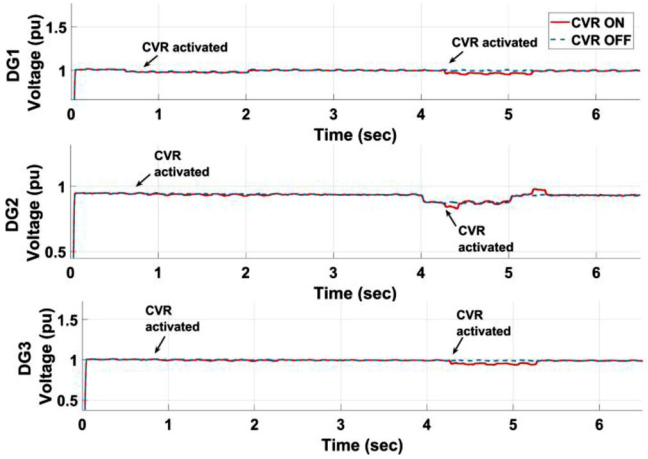

FIGURE 19 Voltage at the PCC.

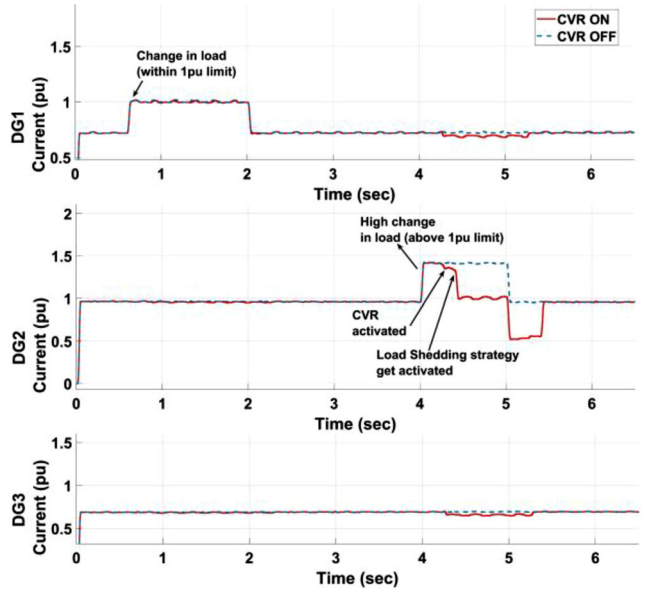

FIGURE 20 Output current of DG.

requires an additional time of 150 ms due to communication delay for sending the command from DG to the EMC and then the required amount of load to be shed at time $t = 4.4$ s. The amount of load to be shed is determined by load shedding strategy and it determined 22.4 kVA of load to be shed from the microgrid to ensure the operation of the microgrid within the tolerable zone ($m_1 \leq \omega_{cvr} \leq 0$ and $0 \leq V_{cvr} \leq m_2$).

The microgrid would still be in power consumption mode due to the given time constraint limit of 0.25 s provided by the H3 signal. Also, on the evaluation of the control strategy with and without CVR, it can be observed from Figures 14 and 20 that the overloading condition of DG 2 prevails without the CVR strategy after shedding 22.4 kVA of non-critical load. Hence, the microgrid needs to perform additional deduction of load to operate within the tolerable zone without the CVR strategy. The circuit breaker disconnects the additional load at time $t = 5$ s and frequency and voltage in the measuring block of

the CVR strategy realize this change which brings the operation of the microgrid as described in (52). As the microgrid reached the normal operating zone, the deactivation of CVR and load-shedding strategy is performed. However, due to the time limit provided to the control scheme, the CVR and load-shedding strategy is disabled at time $t = 5.25$ and 5.4 s respectively.

7 | CONCLUSIONS

The performance of the *P–f* droop and *V–I* droop enabled voltage source inverter is studied and CVR with load shedding approach is demonstrated to operate the VSI in an optimal mode. Along with VSI management, the CVR with the proposed methodology provided convincing results and it effectively demonstrated the retention of power in the range of 14–17% in a stand-alone microgrid. The droop estimation technique for *V–I* droop successfully determined the droop coefficient for *V–I* droop and it ensures proportional sharing of power among DGs. The voltage compensation from the CVR strategy is dependent on the transition of the voltage and frequency of the microgrid and also, and this transition occurred due to a change in the load pattern. It leads to the conclusion that the voltage would be compensated according to the IEEE 1547 specifications and the degree of voltage compensation is dependent on the amount of load variation.

AUTHOR CONTRIBUTIONS

Sumit Kumar Jha and Deepak Kumar: Conceptualization, Writing, Review and Editing, Writing. Prabhat Ranjan Tripathi and Bhargav Appasani: Investigation, Formal Analysis, Supervision. Hossam M. Zawbaa and Salah Kamel: Resources, Writing, Review and Editing

CONFLICT OF INTEREST STATEMENT

The authors declare no conflicts of interest.

DATA AVAILABILITY STATEMENT

The data that support the findings of this study are available from the corresponding author upon reasonable request.

ORCID

Hossam M. Zawbaa https://orcid.org/0000-0001-6548-2993

REFERENCES

1. Krismanto, A.U., Mithulananthan, N., Krause, O.: Stability of renewable energy based microgrid in autonomous operation. Sustainable Energy Grids Networks 13, 134–147 (2018)
2. Jha, S.K., Kumar, D.: Adapting the control strategies of microgrid to propel the future research towards demand side management: A review. In: Reddy, M.J.B., Mohanta, D.K., Kumar, D., Ghosh, D. (eds.) Advances in Smart Grid Automation and Industry 4.0. Lecture Notes in Electrical Engineering, vol 693. Springer, Singapore (2021). https://doi.org/10.1007/978-981-15-7675-1_72
3. Abusara, M.A., Sharkh, S.M., Guerrero, J.M.: Improved droop control strategy for grid-connected inverters. Sustainable Energy Grids Networks 1, 10–19 (2015)
4. Li, Z., Chan, K.W., Hu, J., Guerrero, J.M.: Adaptive droop control using adaptive virtual impedance for microgrids with variable PV outputs and load demands. IEEE Trans. Ind. Electron. 68(10), 9630–9640 (2021). https://doi.org/10.1109/TIE.2020.3022524
5. Zhang, B., Gao, F., Zhang, Y., Liu, D., Tang, H.: An AC-DC coupled droop control strategy for VSC-based DC microgrids. IEEE Trans. Power Electron. 37(6), 6568–6584 (2022). https://doi.org/10.1109/TPEL.2022.3141096
6. Alghamdi, B., Cañizares, C.A.: Frequency regulation in isolated microgrids through optimal droop gain and voltage control. IEEE Trans. Smart Grid 12(2), 988–998 (2021). https://doi.org/10.1109/TSG.2020.3028472
7. Ahmed, K., Seyed mahmoudian, M., Mekhilef, S., Mubarak, N.M., Stojcevski, A.: A review on primary and secondary controls of inverter-interfaced microgrid. J. Mod. Power Syst. Clean Energy 9(5), 969–985 (2021). https://doi.org/10.35833/MPCE.2020.000068
8. Jha, S.K., Kumar, D.: Assessment of battery energy storage system with hybrid renewable energy sources to voltage control of islanded microgrid considering demand-side management capability. Iran. J. Sci. Technol. Trans. Electr. Eng. 44, 861–877 (2020). https://doi.org/10.1007/s40998-019-00273-9
9. Mohamed, Y.A.R.I., El-Saadany, E.F.: Adaptive decentralized droop controller to preserve power sharing stability of paralleled inverters in distributed generation microgrids. IEEE Trans. Power Electron. 23, 2806–2816 (2008)
10. Tayab, U.B., Roslan, M.A.B., Hwai, L.J., Kashif, M.: A review of droop control techniques for microgrid. Renewable Sustainable Energy Rev. 76, 717–727 (2017)
11. Ahmed, M., Meegahapola, L., Vahidnia, A., Datta, M.: Adaptive virtual impedance controller for parallel and radial microgrids with varying X/R ratios. IEEE Trans. Sustainable Energy 13(2), 830–843 (2022). https://doi.org/10.1109/TSTE.2021.3133413
12. Golsorkhi, M.S., Lu, D.D.C.: A control method for inverter-based islanded microgrids based on V–I droop characteristics. IEEE Trans. Power Delivery 30(3), 1196–1204 (2015). https://doi.org/10.1109/TPWRD.2014.2357471
13. Sen, P.K., Lee, K.H.: Conservation voltage reduction technique: An application guideline for smarter grid. IEEE Trans. Ind. Appl. 52(3), 2122–2128 (2016)
14. Ma, Z., Xiang, Y., Wang, Z.: Robust conservation voltage reduction evaluation using soft constrained gradient analysis. IEEE Trans. Power Syst. 37(6), 4485–4496 (2022). https://doi.org/10.1109/TPWRS.2022.3146842
15. Yang, S., Wang, P., Tang, Y., Zhang, L.: Explicit phase lead filter design in repetitive control for voltage harmonic mitigation of VSI-based islanded microgrids. IEEE Trans. Ind. Electron. 64(1), 817–826 (2017)
16. Radwan, A.A.A., Mohamed, Y.A.-R.I., El-Saadany, E.F.: Assessment and performance evaluation of DC-side interactions of voltage-source inverters interfacing renewable energy systems. Sustainable Energy Grids Networks 1, 28–44 (2015)
17. O'Connell, A., Keane, A.: Volt_var curves for photovoltaic inverters in distribution systems. IET Gener., Transmiss. Distrib. 11(3), 730–739 (2017)
18. Wang, Z., Wang, J.: Review on implementation and assessment of conservation voltage reduction. IEEE Trans. Power Syst. 29(3), 1306–1315 (2014)
19. Singh, R., Tuffner, F., Fuller, J., Schneider, K.: Effects of distributed energy resources on conservation voltage reduction (CVR). In: 2011 IEEE Power and Energy Society General Meeting. Detroit, MI, USA, pp. 1–7 (2011)
20. Xu, J., et al.: CVR-based real-time power fluctuation smoothing control for distribution systems with high penetration of PV and experimental demonstration. IEEE Trans. Smart Grid 13(5), 3619–3635 (2022). https://doi.org/10.1109/TSG.2022.3166823
21. Pasha, A.M., Zeineldin, H.H., Al-Sumaiti, A.S., Moursi, M.S.E., Sadaany, E.F.E.: Conservation voltage reduction for autonomous microgrids based on V–I droop characteristics. IEEE Trans. Sustainable Energy 8(3), 1076–1085 (2017)
22. Kahrobaeian, A., Mohamed, Y.A.R.I.: Analysis and mitigation of low-frequency instabilities in autonomous medium-voltage converter based

microgrids with dynamic loads. IEEE Trans. Ind. Electron. 61(4), 1643–1658 (2014)
23. Golsorkhi, M.S., Savaghebi, M.: A decentralized control strategy based on V–I droop for enhancing dynamics of autonomous hybrid AC/DC microgrids. IEEE Trans. Power Electron. 36(8), 9430–9440 (2021). https://doi.org/10.1109/TPEL.2021.3049813
24. Jha, S.K., Kumar, D., Lehtonen, M.: Modified V–I droop based adaptive vector control scheme for demand side management in a stand-alone microgrid. Int. J. Electr. Power Energy Syst. 130, 106950 (2021)
25. Osman, R.: A simple energy-absorbing circuit for current-source inverters. IEEE Trans. Ind. Appl. IA-20(6), 1448–1452 (1984)

How to cite this article: Jha, S.K., Kumar, D., Tripathi, P.R., Appasani, B., Zawbaa, H.M., Kamel, S.: An adaptive vector control method for inverter-based stand-alone microgrids considering voltage reduction and load shedding schemes. IET Gener. Transm. Distrib. 17, 2703–2717 (2023). https://doi.org/10.1049/gtd2.12839